Published in final edited form as:
Mol Cell. 2015 January 8; 57(1): 83–94. doi:10.1016/j.molcel.2014.11.002.

Mitochondrial ADCK3 employs an atypical protein kinase-like fold to enable coenzyme Q biosynthesis

Jonathan A. Stefely[1,7], **Andrew G. Reidenbach**[1,7], **Arne Ulbrich**[2], **Krishnadev Oruganty**[5], **Brendan J. Floyd**[1], **Adam Jochem**[1], **Jaclyn M. Saunders**[3], **Isabel E. Johnson**[1], **Catherine E. Minogue**[2], **Russell L. Wrobel**[3], **Grant E. Barber**[1], **David Lee**[6], **Sheng Li**[6], **Natarajan Kannan**[5], **Joshua J. Coon**[2,4], **Craig A. Bingman**[1,3], and **David J. Pagliarini**[1,3,*]

[1]Department of Biochemistry, University of Wisconsin–Madison, Madison, Wisconsin 53706, USA

[2]Department of Chemistry, University of Wisconsin–Madison, Madison, Wisconsin 53706, USA

[3]Mitochondrial Protein Partnership, University of Wisconsin–Madison, Madison, Wisconsin 53706, USA

[4]Department of Biomolecular Chemistry, University of Wisconsin–Madison, Madison, Wisconsin 53706, USA

[5]Department of Biochemistry, University of Georgia, Athens, Georgia 30602, USA

[6]Department of Medicine and UCSD DXMS Proteomics Resource, University of California San Diego, La Jolla, California 92023, USA

SUMMARY

The ancient UbiB protein kinase-like family is involved in isoprenoid lipid biosynthesis and is implicated in human diseases, but demonstration of UbiB kinase activity has remained elusive for unknown reasons. Here, we quantitatively define UbiB-specific sequence motifs and reveal their positions within the crystal structure of a UbiB protein, ADCK3. We find that multiple UbiB-specific features are poised to inhibit protein kinase activity, including an N-terminal domain that occupies the typical substrate binding pocket and a unique A-rich loop that limits ATP binding by establishing an unusual selectivity for ADP. A single alanine-to-glycine mutation of this loop flips this coenzyme selectivity and enables autophosphorylation, but inhibits coenzyme Q biosynthesis *in vivo*, demonstrating functional relevance for this unique feature. Our work provides mechanistic

[*]Correspondence: pagliarini@wisc.edu.
[7]These authors contributed equally

AUTHOR CONTRIBUTIONS

J.A.S., A.G.R., and D.J.P. conceived of the project and its design. J.A.S., A.G.R., A.U., K.O, B.J.F., A.J., J.M.S., I.E.J., C.E.M., R.L.W, G.E.B., D.L. and C.A.B. performed experiments and data analysis. S.L., N.K., J.J.C., C.A.B. and D.J.P. aided in experimental design. J.A.S., A.G.R., and D.J.P. wrote the manuscript.

ACCESSION NUMBERS

The coordinates and structure factors have been deposited in the Protein Data Bank with accession code 4PED.

insight into UbiB enzyme activity and establishes a molecular foundation for further investigation of how UbiB family proteins affect diseases and diverse biological pathways.

INTRODUCTION

Protein kinase-like (PKL) superfamily members share an active site that catalyzes adenosine triphosphate (ATP)-dependent phosphorylation (Kannan et al., 2007), but evolution of divergent sequence features and unique accessory domains has enabled adoption of a broad range of biological functions. Crystallographic studies have revealed the unique features of 10 of the 20 known PKL families (Hon et al., 1997; Kang et al., 2008; Knighton et al., 1991; Ku et al., 2007; LaRonde-LeBlanc and Wlodawer, 2004; Mao et al., 2008; Walker et al., 1999; Yamaguchi et al., 2001; Young et al., 2003; Zheng and Jia, 2010); however, members of the UbiB family have remained refractory to purification and biochemical analyses.

UbiB kinases are present in archaea, bacteria and eukaryotes (Leonard et al., 1998), and comprise an estimated one-quarter of all microbial PKLs (Kannan et al., 2007). The founding member of the UbiB family, UbiB from *Escherichia coli*, is required for the aerobic biosynthesis of the redox-active lipid ubiquinone, also known as coenzyme Q (CoQ) (Poon et al., 2000). In eukaryotes, UbiB homologs are found exclusively in mitochondria (Pagliarini et al., 2008) and plastids (Lundquist et al., 2012; Lundquist et al., 2013; Martinis et al., 2013), where they have been implicated in stress responses (Jasinski et al., 2008), copper homeostasis (Schlecht et al., 2014), pigmentation (Lundquist et al., 2013), phospholipid metabolism (Tan et al., 2013), and isoprenoid lipid biosynthesis (Do et al., 2001; Lundquist et al., 2013; Martinis et al., 2013).

The human genome contains five UbiB family genes, *ADCK1–5* (Figure 1A). Mutations in ADCK3 and ADCK4 cause a cerebellar ataxia (Horvath et al., 2012; Lagier-Tourenne et al., 2008; Mollet et al., 2008; Pineda et al., 2010) and a steroid-resistant nephrotic syndrome (Ashraf et al., 2013), respectively, that are each associated with CoQ deficiency. Silencing of ADCK1 expression alters epithelial cell migration (Simpson et al., 2008), and silencing of ADCK2 significantly decreases the viability of cells derived from glioblastoma multiforme (Wiedemeyer et al., 2010) and estrogen receptor-positive breast tumors (Brough et al., 2011). As such, ADCK proteins are promising therapeutic targets that await rigorous biochemical characterization.

ADCK3 (CABC1, COQ8), the focus of this work, has been only minimally characterized at the biochemical level. Phylogenetic analyses defined ADCK3 as an ‘atypical kinase’ (Manning et al., 2002) and suggested that ADCK3 and ADCK4 are co-orthologs of the yeast protein Coq8p (Lagier-Tourenne et al., 2008). Coq8p is known to stabilize a complex of CoQ biosynthesis proteins in yeast (He, 2014), but the underlying mechanism is undefined. ADCK3 can weakly rescue the respiratory growth defect of Coq8p knockout (*coq8*Δ) yeast, and this rescue partially restores the phosphorylation state of Coq3p, Coq5p and Coq7p *in vivo*; but, whether this effect is direct or indirect is unknown (Xie et al., 2011). ADCK3 is known to reside in the mitochondrial matrix (Pagliarini et al., 2008; Rhee et al., 2013), and we recently demonstrated that ADCK3 contains a transmembrane domain that can drive homodimerization (Khadria et al., 2014).

The primary gaps in knowledge about the UbiB family center around its undefined enzymatic activity. Although UbiB proteins share some sequence features with protein kinases, whether UbiB proteins actually adopt a PKL fold was unknown. Moreover, previous attempts by our lab and others to demonstrate kinase activity for UbiB proteins *in vitro* were unsuccessful for unknown reasons.

Here, to provide molecular insight into the activity of UbiB family proteins, we integrate bioinformatics, crystallography, *in vitro* activity assays, and investigation of *in vivo* CoQ production. By solving a crystal structure of a UbiB family protein, human mitochondrial ADCK3, we show that UbiB proteins adopt an atypical PKL fold with multiple UbiB-specific features positioned to inhibit protein kinase activity. We demonstrate that mutating one of these unique features relieves enzyme inhibition and enables autophosphorylation *in vitro*, while showing that this same mutation inhibits CoQ production *in vivo*. These results suggest a model wherein inhibition of protein kinase activity is important for the mechanism by which ADCK3 enables CoQ biosynthesis. Our work also suggests a mechanism by which human ADCK3 and ADCK4 mutations disrupt protein stability to cause disease, and provides a foundation for therapeutic targeting of UbiB family proteins.

RESULTS

The UbiB family has numerous unique sequence motifs

The protein kinase-like domain of the UbiB family possesses an N-lobe insert and an N-terminal extension with uncharacterized sequence features (Figure 1A), including a unique and invariant KxGQ motif (Figure 1B). We conducted a statistical analysis of the features that distinguish UbiB proteins from other PKLs, which revealed that the UbiB family also has: an atypical AAAS motif in an alanine-rich (A-rich) loop that replaces the canonical glycine-rich (G-rich) nucleotide-binding loop, an ExD motif in the N-lobe insert, a modified catalytic loop, and a conserved arginine or lysine residue in the F-helix (αF) (Figure 1C and Figure S1A). However, the insolubility of full-length UbiB proteins (Figure S1C) has thus far hampered efforts to determine how these unique sequence elements enable UbiB-specific functions.

Mature mitochondrial ADCK3 is truncated

To generate a tractable system for biochemical analyses, we tested the solubility of various ADCK3 truncation constructs. Mature forms of mitochondrial UbiB proteins are likely processed to remove their mitochondrial targeting sequences (MTS), and they contain predicted single-pass transmembrane (TM) domains that could limit solubility (Figure 1A). However, the MTS of ADCK3 could not be predicted *in silico*, so we determined it experimentally. Immunoblot and Edman degradation analyses of mitochondrial ADCK3 (Figure 1D) immunoprecipitated from human cells revealed that the mature form of ADCK3 is truncated by 162 residues to yield a 55 kDa protein (Figures 1E and 1F)—a size consistent with the observed yeast Coq8p truncation (Vogtle et al., 2009) and the predicted ADCK4 truncation (Figure 1A). Most of the sequence removed upon import into mitochondria lacks conservation among metazoan orthologs (Figure S1B). While the endogenous form of ADCK3 remained refractory to large-scale purification and crystallization, we were able to

purify constructs with N-terminal truncations of 250 residues (ADCK3$^{N\Delta250}$) or 254 residues (ADCK3$^{N\Delta254}$). These constructs retain the PKL domain and the unique N-terminal extension, the combination of which represents the structural core of the UbiB family (Figure 1A). These results, combined with previous localization of ADCK3 to the mitochondrial matrix (Rhee et al., 2013), allowed us to create models for the ADCK3 precursor, the mature mitochondrial form, and the crystallized construct (Figures 1G and 1H).

ADCK3 adopts an atypical protein kinase-like fold

We crystallized and solved the structure of ADCK3$^{N\Delta254}$ at a resolution of 1.6 Å (Figure 2A, Table 1). ADCK3 adopts a core fold similar to that of well-characterized PKLs (Figure S2A), such as protein kinase A (PKA) (Knighton et al., 1991; Zheng et al., 1993) (Figure 2D), whereby the N-lobe folds into a β-sheet and a single α-helix (αC), and the C-lobe folds into a series of α-helices and β-strands. The overall topologies of ADCK3 and PKA are also similar, but ADCK3 contains a long N-terminal extension (GQα1–GQα4), an N-lobe insert between β3 and αC (GQα5–GQα6), and a C-lobe insert between β9 and αF (Cα1–Cα4) (Figures 2C and 2F)— unique features that likely afford UbiB family-specific functions.

Unexpectedly, the N-terminal extension and the N-lobe insert fold into α-helices that pack together and rest directly over the A-rich loop and the PKL cleft, where they place the signature KxGQ motif into the substrate-binding pocket (Figure 2A). We have named this region of ADCK3, composed of the insert and extension, the ‘KxGQ domain’ and its component α-helices ‘GQα1–GQα6’ (Figure 2C). The KxGQ domain completely occludes the cleft that binds peptide substrates in typical protein kinases (Figures 2B and 2E). Moreover, in stark contrast to the architecture of ADCK3, the N-terminal extensions of all other structurally characterized PKL families are positioned far from the active site (Figure S2B–S2K). Even the N-terminal extension and the N-lobe insert of Rio family proteins, which exhibit the highest structural similarity to ADCK3 (Figure S2A), fold away from the nucleotide pocket and leave the PKL cleft open to accept a peptide substrate (Figure S2B).

Within the KxGQ domain of ADCK3, we observed a salt bridge between K276 of the KxGQ motif and E405 of the ExD motif (Figures 3A and 3D). The polar and ionic interactions between Q279, K276, and E405 suggest that they act as a functional triad, which we have named the QKE triad. The QKE triad folds directly into the active site near the A-rich loop and highly conserved PKL residues such as D507 and N493 (Figure 3A). This position of the QKE triad overlaps with that of the substrate phosphoryl acceptor in structures of typical protein kinases. Collectively, this structural analysis of the KxGQ domain and the QKE triad suggests that they could function to inhibit protein kinase activity.

ADCK3 contains an atypical active site

Given that demonstration of kinase activity for a UbiB protein has remained elusive for well over a decade (Leonard et al., 1998), we examined the ADCK3 structure for additional features that could inhibit kinase activity. Comparing the structures of PKA and ADCK3 reveals significant differences within the catalytic loop. In PKA, D166 (D166^{PKA}) is

orientated toward the terminal phosphate of the ATP substrate, where it is thought to act as a catalytic base for the phosphoryl acceptor. In contrast, the homologous ADCK3 residue, $D488^{ADCK3}$, is oriented in the opposite direction, where it forms a bidentate salt bridge with αF through $R611^{ADCK3}$ (Figure 3C and 3E).

While features such as the QKE triad and the D488:R611 salt bridge could inhibit protein kinase activity, our PKA-ADCK3 superposition also shows that ADCK3 has hallmarks of an active kinase, including a salt bridge between K358 and E411 (Figure 3C), cation-binding residues (N493 and D507) poised for catalysis (Figure 3C), and intact kinase 'spines' (Kornev et al., 2006) (Figures S3A and S3B). These hallmark features allow active kinases to bind MgATP and catalyze phosphoryl transfer. ADCK3's retention of these features suggests that it would be capable of performing catalysis following removal of inhibitory constraints, but neither nucleotide binding nor catalytic properties had yet been demonstrated for a UbiB protein.

ADCK3 exhibits an unusual selectivity for binding ADP over ATP

To test whether ADCK3 can bind ATP, we quantified ligand-induced changes in ADCK3 melting temperature (ΔT_m). In the presence of divalent cations, adenine nucleotides significantly stabilized $ADCK3^{N\Delta 250}$, whereas other nucleotides did not (Figure 3F). Surprisingly, ADCK3 exhibited an unusual selectivity for binding ADP over ATP. PKA, an example of a more typical kinase, binds MgATP and MgADP with similar affinity, with dissociation constants of ~10 μM (Bhatnagar et al., 1983). ADP binding could inhibit ATP-dependent kinase activity, so we aimed to define the mechanism by which ADCK3 selectively binds ADP over ATP.

The location of the UbiB-specific KxGQ motif near the active site raises the question of whether it mediates nucleotide binding and determines selectivity for ADP. To measure the effects of ADCK3 point mutations on nucleotide binding, we quantified ΔT_m values over a range of ligand concentrations to generate ligand-binding curves, which allowed us to determine apparent dissociation constants ($K_{d,\,app}$) and maximum ΔT_m values ($\Delta T_{m,\,max}$) (Figure S3C–S3E). As expected, mutation of canonical PKL ATP-binding residues dramatically decreased ATP and ADP binding; however, mutation of the KxGQ motif had minimal effects (Figure 3B), suggesting that it is not part of the core nucleotide-binding pocket.

To further examine the structural basis for nucleotide binding, we used deuterium exchange mass spectrometry (DXMS) (Figure 3G and 3H). DXMS revealed that ADCK3 has a stable hydrophobic core anchored by the F-helix, while the KxGQ domain and portions of the unique C-lobe are more mobile. Dramatic decreases in deuterium exchange rates in the presence of nucleotides were observed for the conserved DFG motif, which coordinates a cation that mediates nucleotide binding (see D507 in Figure 3C), and for the unique A-rich loop. This direct involvement of the UbiB-specific A-rich loop in nucleotide binding nominated it as a possible structural determinant of selectivity for ADP.

The A-rich loop of ADCK3 is a structural determinant of coenzyme selectivity

Comparing the conformation of the A-rich loop of ADCK3 to the G-rich loop of PKA reveals significant differences (Figure 4A). The sterics and conformational flexibility of $G52^{PKA}$ allow a backbone amide of the G-rich loop to hydrogen bond with the γ-phosphate of ATP. The A-rich loop of ADCK3 adopts a different conformation, and the homologous backbone amide is not ideally positioned to bind ATP. Furthermore, in superimposed structures of ADCK3 and PKA, $A339^{ADCK3}$ clashes with the nucleotide bound to PKA.

To test the hypothesis that the A-rich loop of ADCK3 is a determinant of coenzyme selectivity, we mutated its alanine residues to glycine residues, thereby converting it into a more typical G-rich loop. An A339G mutation of ADCK3 significantly enhanced affinity for MgATP without affecting MgADP binding. As such, the A339G mutation affords a 6-fold increase in selectivity for ATP over ADP (K_d^{MgADP}/K_d^{MgATP}) (Figures 4B and S4A). Like the A339G mutation, an A337G,A339G double mutation also enhanced selectively for ATP (Figures 4C and S4A). However, in contrast, an A337G mutation alone did not flip coenzyme selectivity. These results demonstrate that $A339^{ADCK3}$ is a major structural determinant of coenzyme selectivity and suggest that it could also be an important determinant of ADCK3 enzyme activity.

A single A-to-G mutation of the A-rich loop enables autophosphorylation

The G-rich loop of typical protein kinases is important for MgATP binding, peptide substrate binding, and catalysis (Bossemeyer, 1994; Hemmer et al., 1997). To test the idea that the ADCK3 A339G mutation might similarly enable protein kinase activity, we examined the ability of ADCK3 A-rich loop mutants to autophosphorylate. The A339G and A337G,A339G double mutations both enabled autophosphorylation (Figure 4D), which we found to be dependent on time and ATP concentration (Figures 4E–G). MgATP-dependent phosphorylation of the N-terminal serine residue of ADCK3 A339G was also observed by liquid chromatography high-resolution tandem mass spectrometry (LC-MS/MS) (Figure S4B–D). Autophosphorylation was inhibited by an A339G,D507N double mutation (Figure 4H), which also inhibited MgATP binding (Figure 4I), demonstrating that the phosphorylation is ADCK3-dependent and not due to a contaminating kinase. Furthermore, the autophosphorylation was Mg^{2+}-dependent (Figure 4H), a typical feature of kinase activity. Under these reaction conditions, we also observed non-specific phosphorylation of all three ADCK3 variants with MnATP, a result that has been observed previously in reactions with MnATP (Schieven and Martin, 1988). Collectively, these results demonstrate that ADCK3 A339 inhibits protein kinase activity *in vitro*.

Mutation of the conserved KxGQ motif enhances autophosphorylation

The activity of the ADCK3 A339G mutant enabled us to test our structure-based hypothesis that the KxGQ domain inhibits protein kinase activity. In the A339G background, KxGQ motif mutations markedly enhanced autophosphorylation activity (Figure 4J). Interestingly, the enhanced autophosphorylation activity was not observed with KxGQ motif single mutants. Under these conditions, the A339G mutation appears to be necessary for autophosphorylation activity *in vitro*.

In vivo, accessory factors could induce conformational changes of the A-rich loop and the KxGQ domain to enhance activity. Based on our structure, we generated two hypothetical models for how the KxGQ domain could move (Figure S4E). To begin testing these models, we used normal mode analysis (NMA) to examine computationally predicted conformational changes. Subtle harmonic movements of the KxGQ domain were observed by NMA, providing evidence for slight opening of the KxGQ domain as a "3-hinge door" (Figure S4F). Flexibility of "hinge 1," the region between GQα3 and GQα4, would be needed for any opening of the KxGQ domain according to this model—a feature that is supported experimentally by the observation of high B-factors (Figure S4J) and high deuterium exchange rates (Figure 4H) for this region. These techniques cannot provide an indication of how far the KxGQ domain could open; however, collectively, the results suggest that movement of this region is feasible. Even without significant movement of the KxGQ domain, computational analyses predict a small pocket that could potentially accommodate a small phosphoryl acceptor substrate (Figure S4G–I).

UbiB-specific features are required for coenzyme Q biosynthesis

To test the direct functional relevance of novel UbiB family sequence elements, we performed *in vivo* structure-function analyses with Coq8p. Using our ADCK3 structure, we generated a homology model of Coq8p (Figure S5A and S5B), which allowed us to design Coq8p mutations and examine their structural effects. We then expressed Coq8p variants in *coq8*Δ yeast, which exhibit a respiratory growth defect on non-fermentable carbon sources caused by CoQ deficiency. Mutation of conserved nucleotide pocket residues eliminated respiratory growth, both on solid media with non-fermentable carbon sources (Figure 5A) and in liquid media with depleted glucose (Figure S5C). Using high-resolution LC-MS, we demonstrated that these growth phenotypes closely mirrored decreases in CoQ abundance (Figure 5B). Together, this panel of assays enables rapid and precise measurement of the phenotypic effects of mutations to conserved Coq8p and ADCK3 residues.

We next used these yeast assays to define essential residues in the A-rich loop and the KxGQ domain. Importantly, the mutation homologous to ADCK3 A339G, Coq8p A197G, caused a significant decrease in CoQ abundance (Figure 5B), despite its activation of ADCK3 protein kinase activity *in vitro*, demonstrating the functional relevance of this conserved alanine residue. Mutation of the serine residue of the AAAS motif also markedly decreased respiratory growth (Figure 5A) and CoQ abundance (Figure 5B), further emphasizing the importance of the A-rich loop. Finally, mutations of the QKE triad eliminated respiratory growth and CoQ production (Figure 5A and 5B), demonstrating an essential role for the QKE triad in the core function of UbiB proteins.

Pathogenic ADCK3 and ADCK4 mutations disrupt protein stability

Our ADCK3 structure provides an opportunity to investigate the molecular basis of human diseases associated with UbiB family members. ADCK3 mutations that cause a cerebellar ataxia map to multiple regions of the protein, including the KxGQ domain (Figure 6A), further validating the central importance of this unique region of the protein (Horvath et al., 2012; Lagier-Tourenne et al., 2008; Mollet et al., 2008; Pineda et al., 2010). We used our structure to predict the deleterious effects of ADCK3 mutations (Figure 6B), most of which

show decreased protein thermal stability or affinity for nucleotide (Figure 6C and 6D). By generating a homology model of ADCK4, we were likewise able to infer the deleterious effects of mutations in this kinase that cause a kidney disease (Ashraf et al., 2013) (Figure S6).

DISCUSSION

Insights into the enzyme activity of the UbiB family

Since the classification of UbiB family protein sequences as protein kinase-like (Leonard et al., 1998), it has been assumed that UbiB family members are protein kinases. However, until now, to our knowledge, the structure, ligand-binding properties, and activity of a UbiB protein had not been described. Our results demonstrate that a UbiB family protein, ADCK3, does in fact adopt a PKL fold and bind adenine nucleotides in a divalent cation-dependent manner, strengthening the hypothesis that UbiB proteins are *bona fide* kinases.

This work also provides rationale for why demonstration of UbiB protein kinase activity has been so elusive. Our structural and biochemical investigations show that multiple UbiB-specific features inhibit ADCK3 protein kinase activity. With a single A-to-G mutation of the A-rich loop, we were able to release one of these inhibitory mechanisms and demonstrate kinase activity for a UbiB family protein.

Our work also shows that the QKE triad is essential for function *in vivo* and provides insight into the biochemical function of the conserved KxGQ domain. If UbiB proteins catalyze phosphorylation of proteins, as previously hypothesized (Martinis et al., 2013; Xie et al., 2011), then the KxGQ domain is likely to be an autoinhibitory domain because it fills the space normally occupied by peptide or protein substrates in typical protein kinases. This idea is supported by the enhanced autophosphorylation activity of KxGQ mutants in the A339G background. However, our analyses raise a competing hypothesis: ADCK3 may phosphorylate a small molecule, with the KxGQ domain functioning as a substrate-binding domain. This idea is supported by the observation of a potential small molecule binding pocket that could be accessed with minimal conformational changes and would be even more accessible with subtle movements of the KxGQ domain, such as those predicted by our normal mode analysis. The observed phosphorylation of an N-terminal serine is concordant with the protein kinase hypothesis, but this moderately hydrophobic N-terminal sequence could also mimic an elongated small molecule, such as a lipid.

A final hypothesis related to our observation of UbiB-specific inhibitory mechanisms is that ADCK3 is a pseudokinase. However, the retention of all residues necessary for catalysis, and the requirement of these residues for *in vivo* function, suggest that this is unlikely, as all characterized pseudokinases are missing one or more essential catalytic residues (Zeqiraj and van Aalten, 2010).

Implications for our understanding of the PKL superfamily

Our investigation of UbiB family proteins has widespread implications for our understanding of the ubiquitous PKL superfamily. One UbiB-specific feature, the A-rich loop, is a striking deviation from common G-rich nucleotide binding motifs. G-rich motifs

are not only widespread in the PKL superfamily; they are also found in the Rossmann fold (Rossmann et al., 1974) and the p-loop (Walker A motif) (Saraste et al., 1990). Generally, these G-rich motifs enable coordination of nucleotide phosphates by backbone amides. The second glycine in the G-rich loop (Gx**G**xxG) was known to be critical for ATP binding and protein kinase catalysis by PKA (Bossemeyer, 1994; Hemmer et al., 1997), but it was not known what effects this residue had on nucleotide selectivity. Our work demonstrates that the analogous A-rich loop of ADCK3 confers an unusual selectivity for ADP over ATP. Moving forward, it may be important to test the hypothesis that UbiB proteins can use ADP as a phosphoryl donor. An ADP-dependent glucokinase has been described (Ito et al., 2001), but no PKL superfamily members are known to be ADP-dependent kinases.

Insight into the biosynthesis of isoprenoid lipids

Many UbiB family proteins are required for the biosynthesis of isoprenoid lipids, such as coenzyme Q, plastoquinone, phylloquinone (vitamin K), plastochromanol, and α-tocopherol (vitamin E) (Cardazzo et al., 1998; Do et al., 2001; Lundquist et al., 2013; Martinis et al., 2013; Poon et al., 2000). Our work provides a molecular foundation for investigating this requirement. We show that UbiB-specific features, such as the A-rich loop and KxGQ motif, are required for the ability of Coq8p to enable mitochondrial CoQ biosynthesis. Furthermore, our structure-activity investigations suggest that inhibition of protein kinase activity is important for the mechanism by which UbiB proteins enhance coenzyme Q biosynthesis.

Ongoing work in our laboratory seeks to understand why this inhibition of UbiB protein kinase activity is important for isoprenoid lipid metabolism. The yeast ortholog of ADCK3, Coq8p, has an established role in stabilizing a membrane-associated complex of proteins that comprises the CoQ biosynthetic machinery (He et al., 2014), and we currently favor two competing hypotheses for how Coq8p could mechanistically fulfill this role. One hypothesis is that Coq8p is a protein kinase that phosphorylates other proteins in the CoQ complex to stabilize their interactions. If this is true, then our work suggests that this protein kinase activity must be carefully regulated to enable proper phosphorylation of the CoQ complex. However, as detailed above, our work raises the alternative possibility that UbiB proteins are small molecule kinases. If this is true, then Coq8p might phosphorylate a prenyl lipid, which has been suggested to be a part of the mature CoQ biosynthetic complex (He et al., 2014). We recently demonstrated that another CoQ-related protein, COQ9, binds phosphorylated lipids and isoprenoid lipids (Lohman et al., 2014). COQ9 and ADCK3 comprise a single polypeptide in the protozoan, *Tetrahymena thermophila*, suggesting that these proteins might work together to stabilize the CoQ biosynthetic complex or to seed its formation on the inner mitochondrial membrane.

Implications for human diseases involving UbiB family proteins

Mutations of ADCK3 are responsible for a neurodegenerative disease (Horvath et al., 2012; Lagier-Tourenne et al., 2008; Mollet et al., 2008; Pineda et al., 2010), and mutations of a closely related homolog, ADCK4, are responsible for a steroid resistant nephrotic syndrome (Ashraf et al., 2013). The results presented here provide a structural framework for understanding how these ADCK mutations cause human disease.

Other ADCK proteins, such as ADCK2, have been linked to cancer cell viability (Brough et al., 2011; Wiedemeyer et al., 2010), suggesting inhibition of ADCK proteins as a potential therapeutic strategy. Kinases are proven chemotherapeutic targets for small molecule inhibitors, but off-target kinase inhibition can be problematic. Encouragingly, our analyses reveal that the architecture of the UbiB family nucleotide-binding pocket, especially the placement of the KxGQ motif, is likely sufficiently distinct to enable the development of specific inhibitors. Furthermore, ADCK2 has unique sequence features that distinguish it from the other human ADCKs, which should assist development of ADCK2-specific inhibitors. Our structure of ADCK3 provides a foundation for building homology models of ADCK2 for structure-based inhibitor design.

Collectively, our investigation of how ADCK3 uses a significant variation on the PKL fold to enable ubiquinone biosynthesis has broad implications on our understanding of kinase enzyme regulation, catalysis, and substrate recognition. These results also provide a framework for further biochemical analysis and therapeutic targeting of the widespread UbiB family.

EXPERIMENTAL PROCEDURES

Statistical analysis of unique sequence motifs

MAPGAPS (Neuwald, 2009) was used to align over 150,000 sequences belonging to the PKL superfamily, as done previously (Kannan and Neuwald, 2005). The curated alignment was used to delineate uniquely conserved residue patterns in the UbiB family using the program CHAIN (Neuwald, 2007; Neuwald et al., 2003). See Supplemental Experimental Procedures for further details.

Expression and purification of ADCK3$^{N\Delta254}$ for crystallization

Selenomethionine-labeled 8His-MBP-[TEV]-ADCK3$^{N\Delta254}$ was expressed in *E. coli* using IPTG induction essentially as described (Gromek et al., 2013). Protein was purified using a nickel ion metal affinity chromatography (IMAC) column, MBP cleavage by TEV protease (Blommel and Fox, 2007), a second IMAC purification to remove 8His-MBP, and gel filtration. See Supplemental Experimental Procedures for further details.

Crystallization

Crystals of selenomethionine-labeled ADCK3$^{N\Delta254}$ were obtained using the high throughput screening and optimization platform developed at the Center for Eukaryotic Structural Genomics (Markley et al., 2009). Crystallization screens were set with a TTP Labtech Mosquito robot, and a Tecan Genesis was used for optimization solutions. The best crystals were obtained by microseeding into 5 μL of 5 mg/mL selenomethionyl ADCK3$^{N\Delta254}$, 12.5% PEG 3350, 150 mM $(NH_4)_2SO_4$, 5 mM $MgCl_2$, 50 mM NaHEPES pH 7.5.

Expression and purification of ADCK3$^{N\Delta250}$ for *in vitro* assays

8His-MBP-[TEV]-ADCK3$^{N\Delta250}$ was expressed in *E. coli* by autoinduction (Fox and Blommel, 2009). Proteins were purified using cobalt IMAC resin, TEV cleavage, and a

second, subtractive IMAC purification to remove 8His-MBP. See Supplemental Experimental Procedures for further details.

Differential Scanning Fluorimetry (DSF)

ADCK3$^{N\Delta250}$ (1 μM) was mixed with nucleotide and $MgCl_2$ (20 mM) in an aqueous buffer (100 mM HEPES, 150 mM NaCl, pH 7.5) with SYPRO Orange Dye (5X, Life Tech.) (final concentrations), and the fluorescence of the mixture was measured as the temperature was increased from 15 to 99 °C using a Real Time PCR System (Applied Biosystems, ViiA7). The fluorescence data was analyzed with Protein Thermal Shift software (Applied Biosystems) to determine T_m values. See Supplemental Experimental Procedures for further details.

Deuterium exchange mass spectrometry (DXMS)

ADCK3$^{N\Delta250}$ (50 μM) was mixed with $MnCl_2$ (2.5 mM), with or without ATPγS (2 mM) or ADP (2 mM), incubated (20 °C, 20 min), and then cooled to 0 °C. Deuterium exchange was initiated by diluting 2 μL of the ADCK3$^{N\Delta250}$ solution with 10 μL of D_2O buffer (8.3 mM Tris, 150 mM NaCl, in D_2O, pD_{READ} 7.2) at 0 °C. At 10, 100, 1000, 10000, and 100000 s, the exchange reactions were quenched with 18 μL of 3.2 M GuHCl, 0.8% formic acid, 16.6% glycerol. The samples were digested with pepsin and analyzed by LC-MS/MS. The centroids of the isotopic envelopes of nondeuterated, partially deuterated and equilibrium-deuterated peptides were measured using DXMS Explorer (Sierra Analytics Inc., Modesto, CA) and then converted to corresponding deuteration level. See Supplemental Experimental Procedures for further details.

In vitro Kinase Autophosphorylation Assays

Unless otherwise indicated, ADCK3$^{N\Delta250}$ A339G (3 μM) was mixed with [γ-^{32}P]ATP (0.2 μCi/μL, 100 μM $[ATP]_{total}$) and $MgCl_2$ (20 mM) in an aqueous buffer (100 mM HEPES, 150 mM NaCl, pH 7.5) and incubated (37 °C, 100 min) (final concentrations). For the divalent cation screen, $MgCl_2$, $MnCl_2$, or $CaCl_2$ was used at 20 mM. Reactions were quenched with 4xLDS buffer. [γ-^{32}P]ATP was separated from ADCK3 by SDS-PAGE. The gel was stained (Coomassie), dried, and imaged. See Supplemental Experimental Procedures for further details.

Yeast growth assays

Saccharomyces cerevisiae (W303 background strain) *coq8*Δ yeast were transformed with p426 GPD plasmids encoding for Coq8p variants. To assay yeast growth on agar plates, serial dilutions of yeast were dropped onto Ura$^-$ agar media plates containing either glucose (2%, w/v) or glycerol (3%, v/v) and incubated (30 °C, 2 d). To assay yeast growth in liquid media, yeast from a starter culture were swapped into Ura$^-$ media with glucose (0.1%, w/v) and glycerol (3%, v/v) at an initial density of 5×10^6 cells/mL, and growth was monitored by optical density at 600 nm (OD_{600}). See Supplemental Experimental Procedures for further details.

Yeast coenzyme Q (CoQ_6) quantitation by LC-MS

Yeast were grown past the diauxic shift in Ura^- media (10 g/L glucose), isolated by centrifugation, and lysed with glass beads. CoQ_{10} was added as an internal standard. Lipids were extracted and dried under $N_{2(g)}$. LC-MS analysis was performed on a C18 column coupled to a Q Exactive mass spectrometer by a HESI II heated ESI source (Thermo). Quantitation was performed by normalizing peak areas to the CoQ_{10} internal standard. Student's t-test was used to determine statistical significance. See Supplemental Experimental Procedures for further details.

Supplementary Material

Refer to Web version on PubMed Central for supplementary material.

ACKNOWLEDGMENTS

We thank the following members of the UW-Madison-based Mitochondrial Protein Partnership for technical and managerial assistance: Emily Beebe, Tina Misenheimer, Nichole Reinen, Ronnie Frederick, Katarzyna Gromek, Don Drott, David Aceti, John Primm, Brian Fox, and John Markley. We thank Brendan Dolan for microscopy work, Michael Westphall for mass spectrometry support, G.N. Phillips, Jr. for guidance and support in all crystallographic endeavors, Bob Smith and Samir Joshi for crystallomics assistance, and Craig Ogata, Ruslan Sanishvili, Joe Brunzelle and Elena Kondrashkina for beamline support. This work was supported by a Searle Scholars Award, a Shaw Scientist Award and by NIH grants U01GM94622, R01DK098672 and R01GM112057 (to D.J.P.), NIH Ruth L. Kirschstein National Research Service Award F30AG043282 (to J.A.S.), and NIH Chemistry-Biology Interface Training Grant T32GM008505 (to A.G.R.). Use of the Advanced Photon Source was supported by the U.S. DOE (DE-AC02-06CH11357). LS-CAT was supported by the Michigan Economic Development Corporation (085P1000817). GM/CA @ APS has received funds from the NIH NCI (Y1-CO-1020) and NIGMS (Y1-GM-1104).

REFERENCES

Ashraf S, Gee HY, Woerner S, Xie LX, Vega-Warner V, Lovric S, Fang H, Song X, Cattran DC, Avila-Casado C, et al. ADCK4 mutations promote steroid-resistant nephrotic syndrome through CoQ10 biosynthesis disruption. J. Clin. Invest. 2013; 123:5179–5189. [PubMed: 24270420]

Bhatnagar D, Roskoski R Jr. Rosendahl MS, Leonard NJ. Adenosine cyclic 3',5'-monophosphate dependent protein kinase: a new fluorescence displacement titration technique for characterizing the nucleotide binding site on the catalytic subunit. Biochemistry. 1983; 22:6310–6317. [PubMed: 6318814]

Blommel PG, Fox BG. A combined approach to improving large-scale production of tobacco etch virus protease. Protein expression and purification. 2007; 55:53–68. [PubMed: 17543538]

Bossemeyer D. The glycine-rich sequence of protein kinases: a multifunctional element. Trends Biochem. Sci. 1994; 19:201–205. [PubMed: 8048162]

Brough R, Frankum JR, Sims D, Mackay A, Mendes-Pereira AM, Bajrami I, Costa-Cabral S, Rafiq R, Ahmad AS, Cerone MA, et al. Functional viability profiles of breast cancer. Cancer Discov. 2011; 1:260–273. [PubMed: 21984977]

Cardazzo B, Hamel P, Sakamoto W, Wintz H, Dujardin G. Isolation of an Arabidopsis thaliana cDNA by complementation of a yeast abc1 deletion mutant deficient in complex III respiratory activity. Gene. 1998; 221:117–125. [PubMed: 9852956]

Do TQ, Hsu AY, Jonassen T, Lee PT, Clarke CF. A defect in coenzyme Q biosynthesis is responsible for the respiratory deficiency in Saccharomyces cerevisiae abc1 mutants. J. Biol. Chem. 2001; 276:18161–18168. [PubMed: 11279158]

Fox BG, Blommel PG. Autoinduction of protein expression. Curr. Protoc. Protein Sci. 2009 Chapter 5, Unit 5 23.

Gromek KA, Meddaugh HR, Wrobel RL, Suchy FP, Bingman CA, Primm JG, Fox BG. Improved expression and purification of sigma 1 receptor fused to maltose binding protein by alteration of linker sequence. Protein Expr. Purif. 2013; 89:203–209. [PubMed: 23562661]

He CH, Xie LX, Allan CM, Tran UC, Clarke CF. Coenzyme Q supplementation or over-expression of the yeast Coq8 putative kinase stabilizes multi-subunit Coq polypeptide complexes in yeast coq null mutants. Biochim. Biophys. Acta. 2014; 1841:630–644. [PubMed: 24406904]

Hemmer W, McGlone M, Tsigelny I, Taylor SS. Role of the glycine triad in the ATP-binding site of cAMP-dependent protein kinase. J. Biol. Chem. 1997; 272:16946–16954. [PubMed: 9202006]

Hon WC, McKay GA, Thompson PR, Sweet RM, Yang DS, Wright GD, Berghuis AM. Structure of an enzyme required for aminoglycoside antibiotic resistance reveals homology to eukaryotic protein kinases. Cell. 1997; 89:887–895. [PubMed: 9200607]

Horvath R, Czermin B, Gulati S, Demuth S, Houge G, Pyle A, Dineiger C, Blakely EL, Hassani A, Foley C, et al. Adult-onset cerebellar ataxia due to mutations in CABC1/ADCK3. J. Neurol. Neurosurg. Psych. 2012; 83:174–178.

Ito S, Fushinobu S, Yoshioka I, Koga S, Matsuzawa H, Wakagi T. Structural basis for the ADP-specificity of a novel glucokinase from a hyperthermophilic archaeon. Structure. 2001; 9:205–214. [PubMed: 11286887]

Jasinski M, Sudre D, Schansker G, Schellenberg M, Constant S, Martinoia E, Bovet L. AtOSA1, a member of the Abc1-like family, as a new factor in cadmium and oxidative stress response. Plant Physiol. 2008; 147:719–731. [PubMed: 18390807]

Kang J, Yang M, Li B, Qi W, Zhang C, Shokat KM, Tomchick DR, Machius M, Yu H. Structure and substrate recruitment of the human spindle checkpoint kinase Bub1. Mol. Cell. 2008; 32:394–405. [PubMed: 18995837]

Kannan N, Neuwald AF. Did protein kinase regulatory mechanisms evolve through elaboration of a simple structural component? J. Mol. Biol. 2005; 351:956–972.

Kannan N, Taylor SS, Zhai Y, Venter JC, Manning G. Structural and functional diversity of the microbial kinome. PLoS Biol. 2007; 5:e17. [PubMed: 17355172]

Khadria AS, Mueller BK, Stefely JA, Tan CH, Pagliarini DJ, Senes A. A Gly-Zipper Motif Mediates Homodimerization of the Transmembrane Domain of the Mitochondrial Kinase ADCK3. J. Am. Chem. Soc. 2014; 136(40):14068–14077. [PubMed: 25216398]

Kim C, Cheng CY, Saldanha SA, Taylor SS. PKA-I holoenzyme structure reveals a mechanism for cAMP-dependent activation. Cell. 2007; 130:1032–1043. [PubMed: 17889648]

Knighton DR, Zheng JH, Ten Eyck LF, Ashford VA, Xuong NH, Taylor SS, Sowadski JM. Crystal structure of the catalytic subunit of cyclic adenosine monophosphate-dependent protein kinase. Science. 1991; 253:407–414. [PubMed: 1862342]

Kornev AP, Haste NM, Taylor SS, Eyck LF. Surface comparison of active and inactive protein kinases identifies a conserved activation mechanism. Proc. Natl. Acad. Sci. USA. 2006; 103:17783–17788. [PubMed: 17095602]

Ku SY, Yip P, Cornell KA, Riscoe MK, Behr JB, Guillerm G, Howell PL. Structures of 5-methylthioribose kinase reveal substrate specificity and unusual mode of nucleotide binding. J. Biol. Chem. 2007; 282:22195–22206. [PubMed: 17522047]

Lagier-Tourenne C, Tazir M, Lopez LC, Quinzii CM, Assoum M, Drouot N, Busso C, Makri S, Ali-Pacha L, Benhassine T, et al. ADCK3, an ancestral kinase, is mutated in a form of recessive ataxia associated with coenzyme Q10 deficiency. Am. J. Hum. Genet. 2008; 82:661–672. [PubMed: 18319074]

LaRonde-LeBlanc N, Wlodawer A. Crystal structure of A. fulgidus Rio2 defines a new family of serine protein kinases. Structure. 2004; 12:1585–1594. [PubMed: 15341724]

Leonard CJ, Aravind L, Koonin EV. Novel families of putative protein kinases in bacteria and archaea: evolution of the "eukaryotic" protein kinase superfamily. Genome Res. 1998; 8:1038–1047. [PubMed: 9799791]

Lohman DC, Forouhar F, Beebe ET, Stefely MS, Minogue CE, Ulbrich A, Stefely JA, Sukumar S, Luna-Sanchez M, Jochem A, et al. Mitochondrial COQ9 is a lipid-binding protein that associates with COQ7 to enable coenzyme Q biosynthesis. Proc. Natl. Acad. Sci. USA. 2014 doi: 10.1073/pnas.1413128111.

Lundquist PK, Davis JI, van Wijk KJ. ABC1K atypical kinases in plants: filling the organellar kinase void. Trends Plant Sci. 2012; 17:546–555. [PubMed: 22694836]

Lundquist PK, Poliakov A, Giacomelli L, Friso G, Appel M, McQuinn RP, Krasnoff SB, Rowland E, Ponnala L, Sun Q, et al. Loss of plastoglobule kinases ABC1K1 and ABC1K3 causes conditional degreening, modified prenyl-lipids, and recruitment of the jasmonic acid pathway. Plant Cell. 2013; 25:1818–1839. [PubMed: 23673981]

Manning G, Whyte DB, Martinez R, Hunter T, Sudarsanam S. The protein kinase complement of the human genome. Science. 2002; 298:1912–1934. [PubMed: 12471243]

Mao DY, Neculai D, Downey M, Orlicky S, Haffani YZ, Ceccarelli DF, Ho JS, Szilard RK, Zhang W, Ho CS, et al. Atomic structure of the KEOPS complex: an ancient protein kinase-containing molecular machine. Mol. Cell. 2008; 32:259–275. [PubMed: 18951093]

Markley JL, Aceti DJ, Bingman CA, Fox BG, Frederick RO, Makino S, Nichols KW, Phillips GN Jr. Primm JG, Sahu SC, et al. The Center for Eukaryotic Structural Genomics. J. Struct. Funct. Genomics. 2009; 10:165–179. [PubMed: 19130299]

Martinis J, Glauser G, Valimareanu S, Kessler F. A chloroplast ABC1-like kinase regulates vitamin E metabolism in Arabidopsis. Plant Physiol. 2013; 162:652–662. [PubMed: 23632854]

Mollet J, Delahodde A, Serre V, Chretien D, Schlemmer D, Lombes A, Boddaert N, Desguerre I, de Lonlay P, de Baulny HO, et al. CABC1 gene mutations cause ubiquinone deficiency with cerebellar ataxia and seizures. Am. J. Hum. Genet. 2008; 82:623–630. [PubMed: 18319072]

Neuwald AF. The CHAIN program: forging evolutionary links to underlying mechanisms. Trends Biochem. Sci. 2007; 32:487–493. [PubMed: 17962021]

Neuwald AF. Rapid detection, classification and accurate alignment of up to a million or more related protein sequences. Bioinformatics. 2009; 25:1869–1875. [PubMed: 19505947]

Neuwald AF, Kannan N, Poleksic A, Hata N, Liu JS. Ran's C-terminal, basic patch, and nucleotide exchange mechanisms in light of a canonical structure for Rab, Rho, Ras, and Ran GTPases. Genome Res. 2003; 13:673–692. [PubMed: 12671004]

Pagliarini DJ, Calvo SE, Chang B, Sheth SA, Vafai SB, Ong SE, Walford GA, Sugiana C, Boneh A, Chen WK, et al. A mitochondrial protein compendium elucidates complex I disease biology. Cell. 2008; 134:112–123. [PubMed: 18614015]

Pineda M, Montero R, Aracil A, O'Callaghan MM, Mas A, Espinos C, Martinez-Rubio D, Palau F, Navas P, Briones P, et al. Coenzyme Q(10)-responsive ataxia: 2-year-treatment follow-up. Mov. Disord. 2010; 25:1262–1268. [PubMed: 20629161]

Poon WW, Davis DE, Ha HT, Jonassen T, Rather PN, Clarke CF. Identification of Escherichia coli ubiB, a gene required for the first monooxygenase step in ubiquinone biosynthesis. J. Bacteriol. 2000; 182:5139–5146. [PubMed: 10960098]

Rhee HW, Zou P, Udeshi ND, Martell JD, Mootha VK, Carr SA, Ting AY. Proteomic mapping of mitochondria in living cells via spatially restricted enzymatic tagging. Science. 2013; 339:1328–1331. [PubMed: 23371551]

Rossmann MG, Moras D, Olsen KW. Chemical and biological evolution of nucleotide-binding protein. Nature. 1974; 250:194–199. [PubMed: 4368490]

Saraste M, Sibbald PR, Wittinghofer A. The P-loop--a common motif in ATP- and GTP-binding proteins. Trends Biochem. Sci. 1990; 15:430–434. [PubMed: 2126155]

Schieven G, Martin GS. Nonenzymatic phosphorylation of tyrosine and serine by ATP is catalyzed by manganese but not magnesium. J. Biol. Chem. 1988; 263:15590–15593. [PubMed: 3139672]

Schlecht U, Suresh S, Xu W, Aparicio AM, Chu A, Proctor MJ, Davis RW, Scharfe C, St Onge RP. A functional screen for copper homeostasis genes identifies a pharmacologically tractable cellular system. BMC genomics. 2014; 15:263. [PubMed: 24708151]

Simpson KJ, Selfors LM, Bui J, Reynolds A, Leake D, Khvorova A, Brugge JS. Identification of genes that regulate epithelial cell migration using an siRNA screening approach. Nat. Cell Biol. 2008; 10:1027–1038. [PubMed: 19160483]

Tan T, Ozbalci C, Brugger B, Rapaport D, Dimmer KS. Mcp1 and Mcp2, two novel proteins involved in mitochondrial lipid homeostasis. J. Cell Sci. 2013; 126:3563–3574. [PubMed: 23781023]

Vogtle FN, Wortelkamp S, Zahedi RP, Becker D, Leidhold C, Gevaert K, Kellermann J, Voos W, Sickmann A, Pfanner N, et al. Global analysis of the mitochondrial N-proteome identifies a processing peptidase critical for protein stability. Cell. 2009; 139:428–439. [PubMed: 19837041]

Walker EH, Perisic O, Ried C, Stephens L, Williams RL. Structural insights into phosphoinositide 3-kinase catalysis and signalling. Nature. 1999; 402:313–320. [PubMed: 10580505]

Wiedemeyer WR, Dunn IF, Quayle SN, Zhang J, Chheda MG, Dunn GP, Zhuang L, Rosenbluh J, Chen S, Xiao Y, et al. Pattern of retinoblastoma pathway inactivation dictates response to CDK4/6 inhibition in GBM. Proc. Natl. Acad. Sci. USA. 2010; 107:11501–11506. [PubMed: 20534551]

Xie LX, Hsieh EJ, Watanabe S, Allan CM, Chen JY, Tran UC, Clarke CF. Expression of the human atypical kinase ADCK3 rescues coenzyme Q biosynthesis and phosphorylation of Coq polypeptides in yeast coq8 mutants. Biochim. Biophys. Acta. 2011; 1811:348–360. [PubMed: 21296186]

Yamaguchi H, Matsushita M, Nairn AC, Kuriyan J. Crystal structure of the atypical protein kinase domain of a TRP channel with phosphotransferase activity. Mol. Cell. 2001; 7:1047–1057. [PubMed: 11389851]

Young TA, Delagoutte B, Endrizzi JA, Falick AM, Alber T. Structure of Mycobacterium tuberculosis PknB supports a universal activation mechanism for Ser/Thr protein kinases. Nat. Struct. Mol. Biol. 2003; 10:168–174.

Zeqiraj E, van Aalten DM. Pseudokinases-remnants of evolution or key allosteric regulators? Curr. Opin. Struct. Biol. 2010; 20:772–781. [PubMed: 21074407]

Zheng J, Jia Z. Structure of the bifunctional isocitrate dehydrogenase kinase/phosphatase. Nature. 2010; 465:961–965. [PubMed: 20505668]

Zheng J, Trafny EA, Knighton DR, Xuong NH, Taylor SS, Ten Eyck LF, Sowadski JM. 2.2 A refined crystal structure of the catalytic subunit of cAMP-dependent protein kinase complexed with MnATP and a peptide inhibitor. Acta Crystallogr. D. 1993; 49:362–365. [PubMed: 15299527]

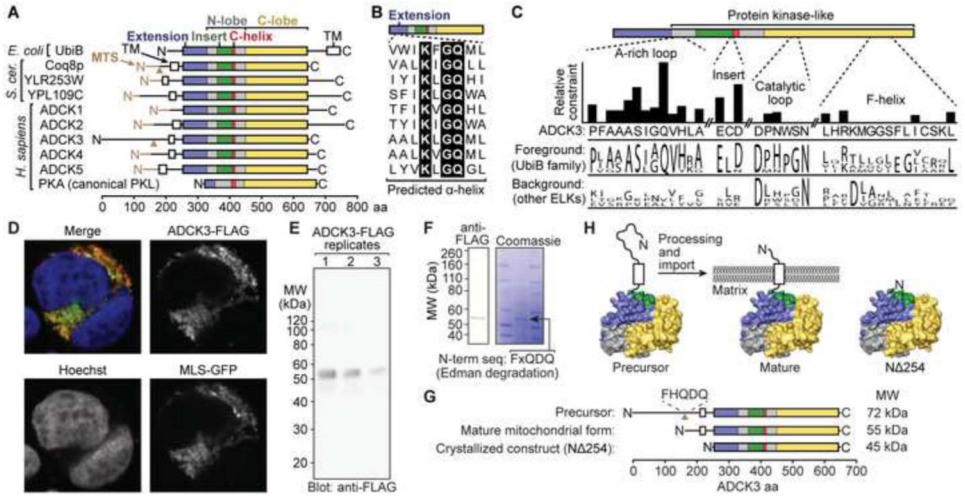

Figure 1. Unique sequence features of the UbiB family and ADCK3

(**A**) Domain structures of UbiB family proteins (human, yeast, and *E. coli*) and PKA (human). Brown triangles represent observed N-termini of mature Coq8p and mature ADCK3 (see D–G).

(**B**) Alignment of a predicted α-helix in the N-terminal extension of UbiB family proteins as listed in (A).

(**C**) Signature motifs identified by a statistical analysis of the UbiB family (foreground) compared to other ePK-like kinase (ELK) sequences (background) with associated sequence logos. Histogram bar height (on an approximately logarithmic scale) represents the selective constraint imposed on unique foreground residue (a measure of “uniqueness”). See also Figure S1A.

(**D**) Confocal microscopy of HEK293 cells transfected with ADCK3-FLAG and MLS-GFP (mitochondrial marker). Nuclear DNA is visualized by Hoechst stain.

(**E**) Anti-FLAG immunoblot of ADCK3-FLAG immunopreciptated from HEK293 cells (3 biological replicates).

(**F**) N-terminal sequence (FxQDQ) of a Coomassie-stained band of mature, IP’d ADCK3-FLAG at ~55 kDa as determined by Edman degradation (‘x’ indicates an unclear residue), and a parallel lane analyzed by anti-FLAG immunoblot.

(**G**) Domain structures of precursor, mature, and crystallized ADCK3. The location of the observed mitochondrial ADCK3-FLAG N-terminus (FHQDQ) in the full-length protein is indicated, along with the predicted molecular weights of all three proteins. See also Figure S2.

(**H**) Cartoon models of precursor, mature and crystallized ADCK3. The NΔ254 model is based on our crystal structure (see Figure 2).

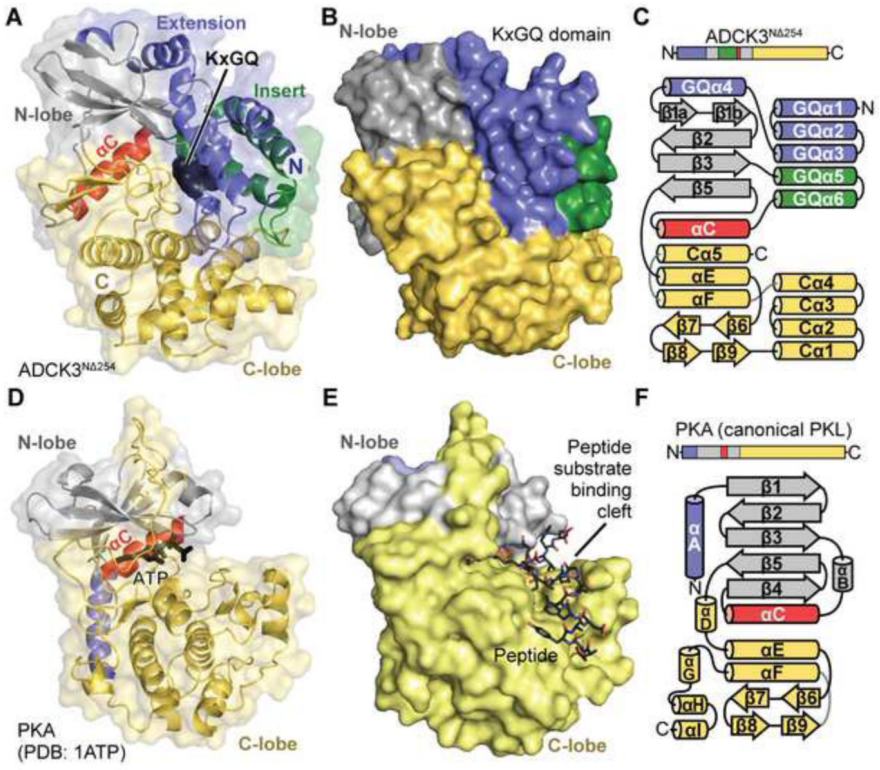

Figure 2. X-ray crystal structure of ADCK3^{NΔ254}

(**A**) Overall structure of ADCK3^{NΔ254} with domains colored as in Figure 1A and the KxGQ motif residues represented with black spheres.

(**B**) Surface representation of ADCK3^{NΔ254} with domains colored as in (A).

(**C**) Topology map of ADCK3^{NΔ254} colored as in (A).

(**D**) Overall structure of PKA (PDB: 1ATP) (Zheng et al., 1993) with domains colored as in Figure 1A and bound ATP represented with black sticks.

(**E**) Surface representation of PKA with a peptide substrate analog represented as sticks and domains colored as in (D).

(**F**) Topology map of PKA colored as in (D).

See also Figure S2.

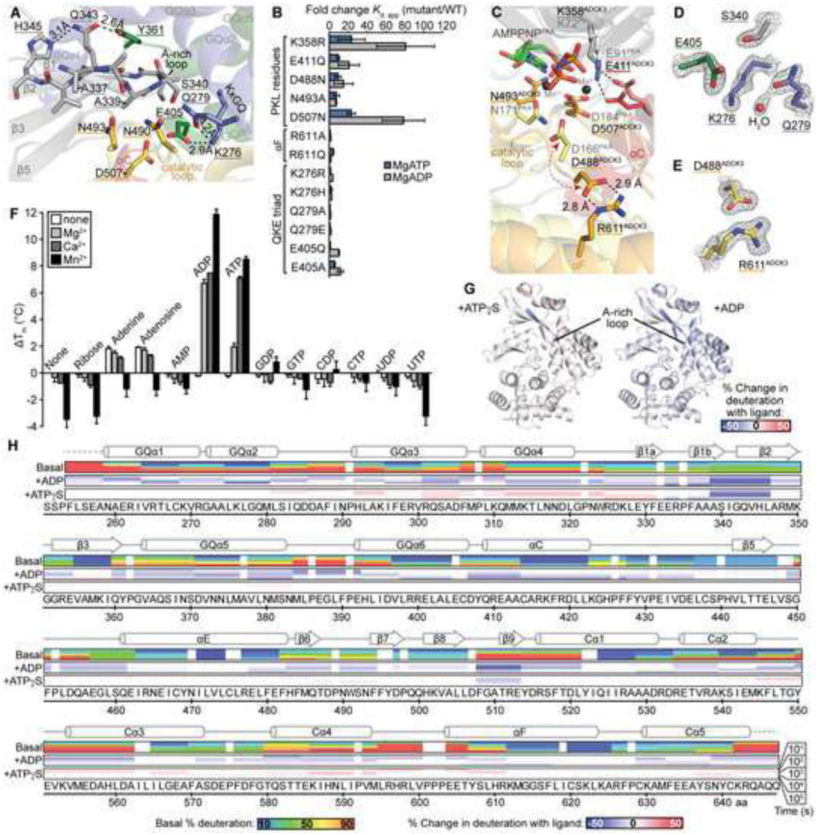

Figure 3. ADCK3 adopts an atypical PKL active site that binds nucleotides

(**A**) Structure of the A-rich loop and the QKE triad of ADCK3$^{N\Delta254}$ colored as in Figure 2.

(**B**) Fold changes in apparent $K_d^{Mg\text{-}ATP}$ and $K_d^{Mg\text{-}ADP}$ for ADCK3$^{N\Delta250}$ mutants compared to wild type as assessed by differential scanning fluorimetry (DSF) (mean ± s.d., n = 3).

(**C**) Superposition of the nucleotide binding pockets of ADCK3$^{N\Delta254}$ (darker colors and black text) and PKA (PDB: 2QCS) (Kim et al., 2007) (lighter colors and gray text) colored as in Figure 2. The nucleotide (AMPPNP) (green) and cations (black spheres) are from the PKA structure. Red arrows highlight the unusual conformation of D488^{ADCK3}.

(**D**) Simulated annealing composite omit maps ($2mF_o$–DF_c) contoured at 1.4σ (gray mesh) of the QKE triad and the serine of the AAAS motif.

(**E**) Simulated annealing composite omit map ($2mF_o$–DF_c) of D488 and R611 contoured at 1.8σ (gray mesh).

(**F**) ΔT_m of ADCK3$^{N\Delta250}$ due to addition of various ligands and cations (mean ± s.d., n = 3 independent ΔT_m determinations).

(**G**) Average differences (over 5 time points) in deuterium exchange of ADCK3$^{N\Delta250}$ due to the presence of ATPγS or ADP mapped onto the structure of ADCK3$^{N\Delta254}$.

(**H**) Ribbon maps of ADCK3 showing deuterium exchange levels in three separate conditions (Basal, Mn^{2+} only; +ADP, MnADP; +ATPγS, MnATPγS) at five separate time points. Conditions with MnADP and MnATPγS are shown as changes in deuteration compared to the basal levels for each time point. Incubation times with D_2O are shown at the bottom right.

See also Figure S3.

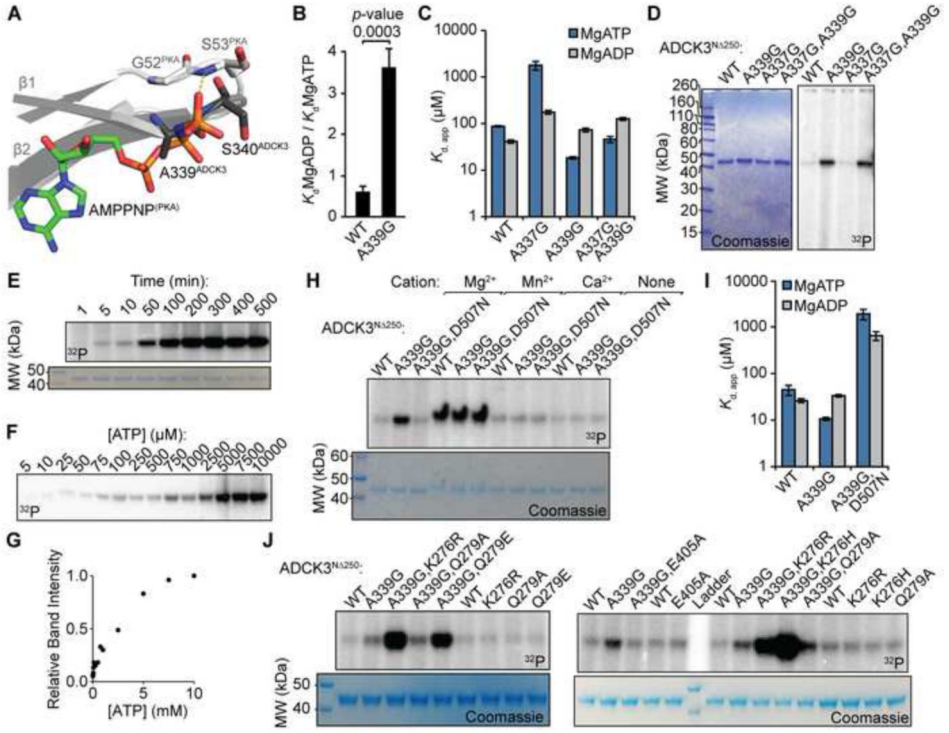

Figure 4. A single A-to-G mutation of the A-rich loop flips nucleotide selectivity and enables ADCK3 autophosphorylation

(**A**) Comparison of the G-rich loop of PKA (PDB: 2QCS) and the A-rich loop of ADCK3$^{N\Delta254}$ (dark gray). AMPPNP (green) is from the PKA structure. The overall structural superposition is the same as in Figure 3C.

(**B**) Nucleotide selectivity of ADCK3$^{N\Delta250}$ A339G compared to wild type (WT). Apparent K_d values were assessed by DSF (mean ± s.d., n = 3; 3 independent K_d measurements were made for each of 3 different protein preparations of WT and A339G).

(**C and I**) $K_d^{Mg\text{-}ATP}$ and $K_d^{Mg\text{-}ADP}$ for ADCK3$^{N\Delta250}$ variants as assessed by DSF (mean ± s.d., n = 3 independent K_d determinations).

(**D, E, F, H, J**) SDS-PAGE analysis of *in vitro* [γ-^{32}P]ATP autophosphorylation reactions with ADCK3$^{N\Delta250}$ variants. MgATP was used for all reactions except those noted in (H).

(**E**) Time course of ADCK3$^{N\Delta250}$ A339G autophosphorylation.

(**F**) Dependence of ADCK3$^{N\Delta250}$ A339G autophosphorylation on ATP concentration.

(**G**) Relative quantification of radioactivity from ^{32}P-ADCK3$^{N\Delta250}$ A339G bands in (F).

See also Figure S4.

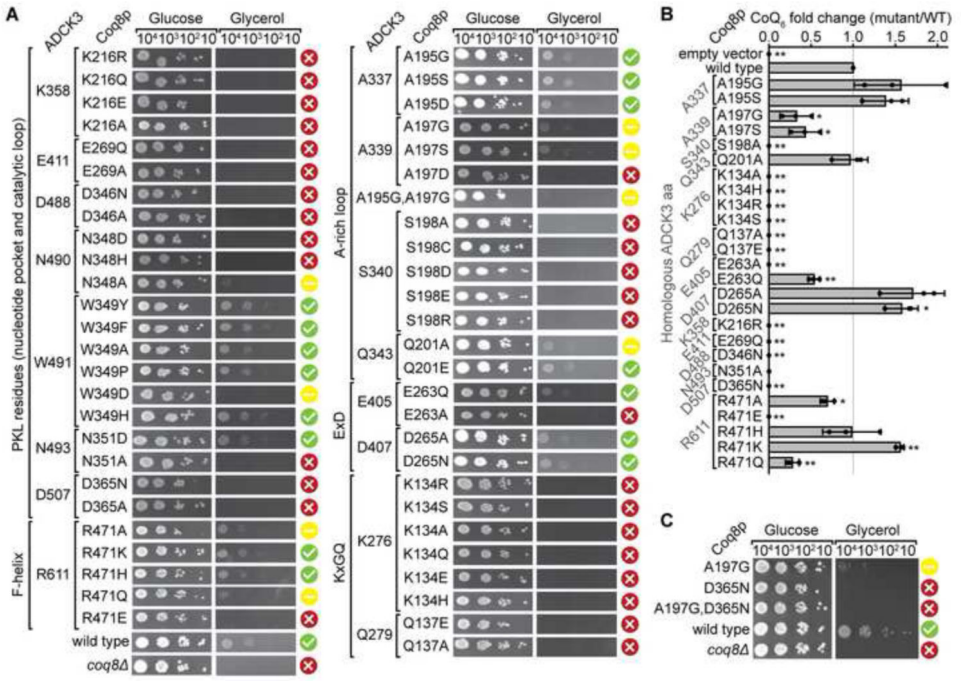

Figure 5. UbiB-specific features of Coq8p are required for yeast growth and CoQ biosynthesis

(**A and C**) Serial dilutions of yeast transformed with the indicated Coq8p variants grown on agar plates with glucose or glycerol. Homologous ADCK3 residues are indicated to the left of the Coq8p residues. Red 'X' symbols indicate no growth on glycerol, yellow dash symbols indicate moderate or low growth on glycerol, and green check mark symbols indicate wild type-like growth on glycerol.

(**B**) Fold changes in CoQ_6 abundance of yeast with Coq8p point mutations compared to wild type Coq8p as determined by LC-MS (mean with 95% c.i., n = 3 biological replicates).

See also Figure S5.

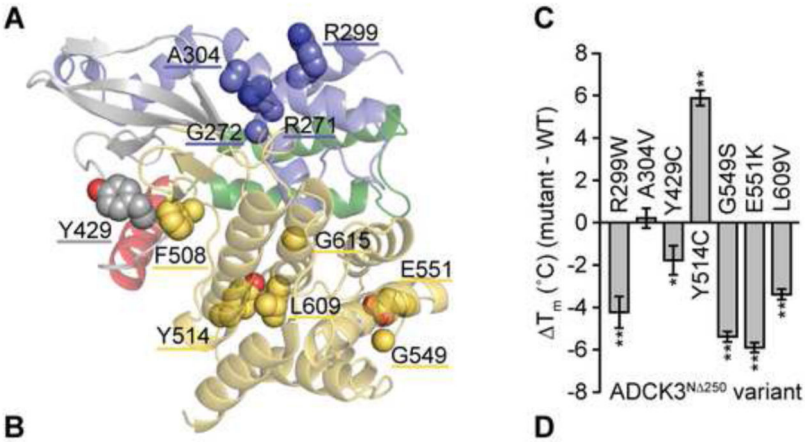

B

Mutation	Predicted effects on ADCK3 structure
R271C	Loss of interactions with V300 and Y361
G272V	Steric clash with I341 and S340
G272D	Steric clash with I341 and S340
R299W	Loss of interactions with S303 and E261
A304V	Steric clash with P335 and A338
A304T	Steric clash with P335 and A338
Y429C	Loss of interactions with E446 & R419
F508S	Altered DFG motif conformation
Y514C	Loss of H-bond with E605 backbone
G549S	Steric clash with I542
E551K	Loss of H-bond with T548 backbone
L609V	Altered F-helix conformation
G615D	Altered F-helix conformation

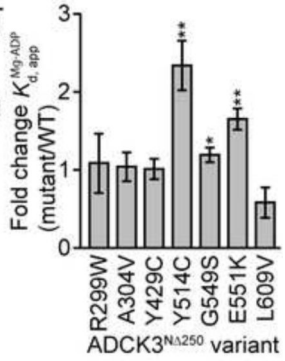

Figure 6. Pathogenic ADCK3 mutations disrupt protein stability

(**A**) Residues mutated in patients with cerebellar ataxia mapped onto the ADCK3$^{N\Delta254}$ structure as spheres. Domains are colored as in Figure 2.

(**B**) Predicted structural effects of pathogenic ADCK3 mutations.

(**C**) Fold changes in ΔT_m of ADCK3$^{N\Delta250}$ mutants compared to wild type as assessed by DSF (mean ± s.d., n = 3 independent ΔT_m determinations).

(**D**) Fold changes in apparent K_d^{MgADP} for ADCK3$^{N\Delta250}$ mutants compared to wild type as assessed by DSF (mean ± s.d., n = 3 independent $K_{d,\,app}$ determinations). *p-value < 0.05, **p-value < 0.01.

Table 1

X-ray data collection and refinement statistics.

Data collection	
Space group	C 1 2 1
Cell dimensions	
a, *b*, *c* (Å)	148.671, 54.557, 45.009
αβγ(°)	90, 94, 90
Resolution (Å)	39.63–1.639 (1.697–1.639)[a]
R_{sym} or R_{merge}	0.0954 (0.862)
$I/\sigma I$	22.9 (1.9)
Completeness (%)	93.2 (79.5)
Redundancy	7.6 (5.6)
Refinement	
Resolution (Å)	39.63–1.639
No. reflections	324414 (24751)
R_{work}/R_{free}	0.1649/0.2110
No. atoms	
Protein	3213
Ligand/ion	10
Water	267
B-factors	
Protein	19.3
Ligand/ion	26.9
Water	25.4
R.m.s. deviations	
Bond lengths (Å)	0.012
Bond angles (°)	1.43

[a]Highest resolution shell is shown in parenthesis.